Original Article	*Curr. Appl. Sci.*, **2025**, *3*(2):61-72 DOI: 10.22034/cas.2025.496057.1045	Current Applied Sciences

Optimization of the State of an Inverted Pendulum System Using Kalman Filter in the Presence of Gaussian and Poisson Noise

Mohammadreza Pourmir

Computer Engineering Department, Faculty of Engineering, University of Zabol, Zabol, Iran

Corresponding author's e-mail: *pormir@uoz.ac.ir*

Article Information

Received: 26 December 2024
Revised: 31 January 2025
Accepted: 06 February 2025
Published online: 12 April 2025

Keywords

Extended Kalman filter
Inverted pendulum system
Kalman filter
Random noise

Abstract

The inverted pendulum problem is an interesting equilibrium problem because the uncontrolled system is unstable and if the base does not move to maintain the vertical position, the pendulum will simply fall and its dynamics are also nonlinear. The Kalman filter is a set of mathematical equations that provides an efficient computational (recursive) solution of the least squares' method. The Kalman filter supports the estimation of past, present, and even future states, and can perform the estimation well even when the exact nature of the modeled system is unknown. This paper aims to estimate the state of the system to optimize the state created by the base in the inverted pendulum problem model so that the pendulum remains in the upright state. The generated random noise signals are added to the real measurement data generated using the system dynamics and these data are used to estimate the system states using the Kalman filter and the extended Kalman filter. The results of these estimates are analyzed and compared.

1. Introduction

Because of its nonlinear, unstable, and non-minimum phase dynamics, the inverted pendulum system (IPS) has long been of interest for stabilization and control. Environmental elements and disturbances are the factors that affect the system, and this has made controlling the system a complex challenge. This system is a widely utilized control problem at research institutes worldwide for teaching linear and nonlinear control theories linked to mechanical systems with nonlinear dynamics, robotics, missiles, air vehicles, and spacecraft [1, 2]. For pathways with varying radii, a particular kind of system is employed to regulate a motorcycle's balance while it rotates.

The inverted pendulum system was initially studied in 1908 [3], but between that year and 1960, there was hardly any literature on the topic. Some tall, thin buildings survived the 1960 Chilean earthquake, although other seemingly stable buildings suffered significant damage. As a result, several academics looked more closely to find

a good answer [4]. It was found that there is an unexpected scaling effect that makes the large block more stable than the small block among two blocks of similar geometry. The earthquake-induced pendulum structure was modeled as a rigid base block system, and the block overturning was converted into the studied system by applying horizontal acceleration, sinusoidal pulses, and seismic-type excitations. Furthermore, tall blocks that are subjected to horizontal forces during earthquakes have increased stability. Since then, as contemporary control theory has advanced, a variety of control techniques, including proportional-integral-derivative control, cloud model control, fuzzy control, sliding mode control, and neural network control techniques, have been applied to various kinds of IPSs [5-7]. These techniques offer several approaches to IPS control.

The authors of [8] suggested a reliable optimum control technique for linear systems with matched uncertainty. Nevertheless, the scenario in which the matched condition's ambiguity is not taken into account. Resilient optimum control of uncertain systems was studied by Lin et al. [9, 10] by solving a Riccati algebraic equation (RAE) and varying the weighting matrix value to produce resilient control rules. A unified approach was introduced by Zhang et al. [11] for the analysis of resilient optimum control problems with a customizable uncertainty set. For robust optimal control of a class of uncertain dependent nonlinear systems with matching uncertainties, Wang et al. [12] created a novel adaptive critical learning approach. They also created data-driven adaptive critical schemes to solve the Hamilton-Jacobi-Bellman (HJB) equation associated with the transformed optimal control problem. Indeed, dynamic programming [13] and maximum principles [14] are the two basic approaches used to solve optimal control issues. It is possible to solve the system's HJB equation using the dynamic programming approach. Either a continuous or discrete system will ultimately solve an RAE when dealing with the optimal control issue of a linear system with a quadratic performance index. However, the dynamic programming method is employed to solve the optimal control problem when the state vector or control input vector in the dynamic system has a large dimension [15].

2. State of the Problem

To keep the pendulum in the upright position based on the base state, the goal of this work is to estimate the system state to optimize it. The actual measurement data produced by the system dynamics is supplemented with the generated random noise signals, such as Gaussian and Poisson noise. The system states are then estimated using the Kalman filter and the extended Kalman filter, and the outcomes of these estimations are examined and contrasted. A variety of controllers are tested and experimented with using the IPS because of its nonlinearity, instability, and non-minimum phase properties. The following is this system's equation of motion (1):

$$(M+m)\ddot{x} + b\dot{x} + ml\ddot{\theta}cos\theta - ml\dot{\theta}^2 sin\theta = F \tag{1}$$

$$(I+ml^2)\theta + mglsin\theta = -ml\ddot{x}cos\theta$$

where M is the base's weight, m is the pendulum's weight, b is the base's coefficient of friction, l is the pendulum's length to its center of mass, I is its mass moment of inertia, F is the force applied to the base, x is the base's coordinate, and θ is the pendulum's angle from the perpendicular (Figure 1).

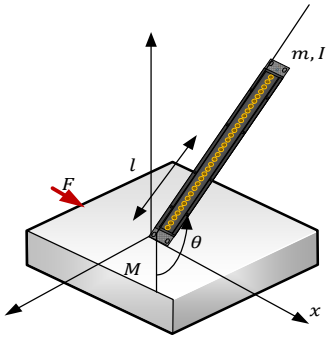

Figure 1. Inverted pendulum model

The ODE equation for this continuous nonlinear system is as follows (2):

$$\dot{X} = F(x_{eq}, u_{eq}) = 0 \tag{2}$$

Around the equilibrium point $\theta = \pi$, it becomes linear. According to the state space model, which depicts a physical system using inputs, outputs, and states, the constant-time linear continuous system is as follows (3):

$$\dot{X} = Ax + Bu \tag{3}$$

$$Y = Cx + Du$$

In this case, the state vector is denoted by x, the output by Y, the input by u, the state matrix by A, the output by C, the feedforward by D, and the derivative of the state vector by $\dot{X}$ Calculating the Jacobian of $f(x,u)$ concerning x and u yields the matrices A and B, whereas calculating the Jacobian of $h(x,u)$ for x and u at the equilibrium points and elsewhere yields the matrices C and D (4). The state space scheme looks like this:

$$X = \begin{bmatrix} x \\ v \\ \theta \\ w \end{bmatrix} \tag{4}$$

where the pendulum's base velocity is $v = \dot{x}$ and its angular velocity is $w = \dot{\theta}$.The model is linearized around the equilibrium point $\theta = \pi$ to get this state space model. By linearizing the equations of motion around the equilibrium point, the matrix A is produced, which is provided by:

$$A = \begin{bmatrix} 0 & 1 & 1 & 0 \\ 0 & \dfrac{-\left(I + ml^2\right)b}{p} & \dfrac{m^2 g l^2}{p} & 0 \\ 0 & 0 & 0 & 1 \\ 0 & \dfrac{-mlb}{p} & \dfrac{mgl(M+m)}{p} & 0 \end{bmatrix} \tag{5}$$

And matrices $B, C, and\ D$:

$$B = \begin{bmatrix} 0 \\ \dfrac{-(I + ml^2)}{p} \\ 0 \\ \dfrac{ml}{p} \end{bmatrix} \tag{6}$$

$$C = \begin{bmatrix} 1 & 0 & 0 & 0 \\ 0 & 0 & 1 & 0 \end{bmatrix} \tag{7}$$

$$D = \begin{bmatrix} 0 \\ 0 \end{bmatrix} \tag{8}$$

where p is considered as follows

$$p = I(M + m) + Mml^2$$

The system's states are shown in the matrix X. The base position and angular position of the pendulum are the system outputs, while the scalar u that regulates the base velocity and angular velocity of the pendulum are the system inputs. The output function looks like this:

$$Y = h(x, u) \tag{9}$$

The controllability and observability matrices are calculated as follows:

```
mu = [1 0 0.1 0]';
x(:,1) = mu;
u =0;
xreal(:,1) = mu;
for i=1 :100
     xreal(:,i+1) = A*(xreal(:,i))+B*u;
     yreal(:,i) = C*(xreal(:,i));
end
```

In the noisy mode, the state and output equations are as follows:

```
R = [.2 0;
      0 .2];
G=eye(4);
H = [1 0;0 1];
sigma = eye(4);
mu = [1 0 0.1 0]';
x(:,1) = mu;
u =0;
wn=
[normrnd(0,0.1,100,1),normrnd(0,0.2,100,1),normrnd(0,0.1,100,1),normrnd(0,0.3,100,1)];
for i=1 :100
     x(:,i+1) = A*(x(:,i))+B*u + (G*w(i,:)');
     y(:,i) = C*x(:,i) + H*v(i,:)';
end
```

The system has full rank controllability and observability matrices, and we have:

$$\boldsymbol{O} = \begin{bmatrix} 1 & 0 & 0 & 0 \\ 0 & 0 & 1 & 0 \\ 0 & 1 & 0 & 0 \\ 0 & 0 & 0 & 1 \\ 0 & -0.6667 & 0.3333 & 0 \\ 0 & -0.333 & 0.6667 & 0 \\ 0 & 0.444 & -0.222 & 0333 \\ 0 & 0.222 & -0.1111 & 0.6667 \end{bmatrix} \tag{10}$$

In a real prediction loop, the Kalman filter functions. The Kalman filter, once initiated, offers the uncertainty of the forecast as well as the condition of the system in the subsequent step. The Kalman filter modifies or updates the current state's prediction and uncertainty upon measurement. A detailed illustration of how the Kalman filter works is shown in Figure 2.

The two phases of the Kalman filter's operation are prediction and correction. Every filter model is predicated on the behavior of the system that employs it. The Kalman filter finds the most likely state by combining the data from the measurement and the guess. The Kalman filter is optimal in specific situations, meaning that it can reduce the error between the updated guess and the actual state. This type of Kalman filter is known as a linear Kalman filter since it operates with linear models. The ability to apply such a filter to any signal or variable that exhibits

linear change over time is known as linearity. It is demonstrated that Kalman filters are best when the measurement data and process noise have a normal distribution.

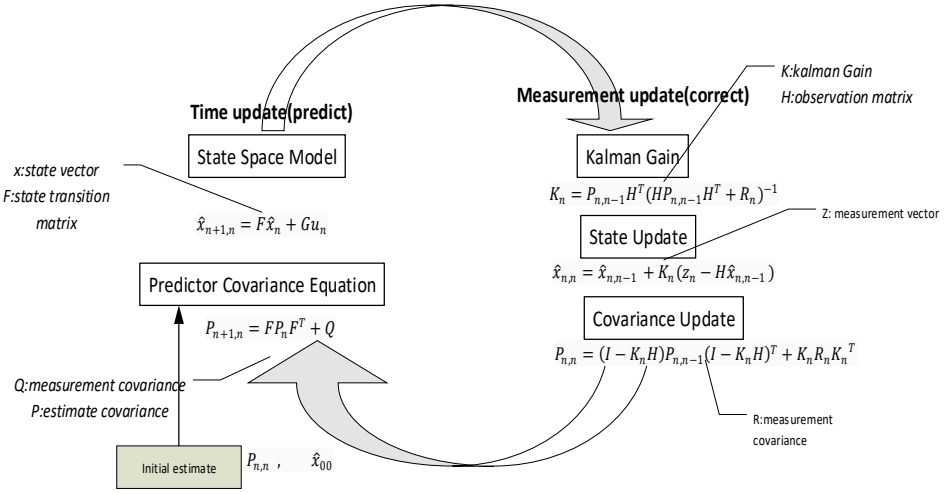

Figure 2. Kalman filter operation

A straightforward concept underlies the magic of Kalman: the joint probability of the two normal distributions stays normal as both the sensor readings and the best estimate come from a normal distribution. Once again, the new best estimate is normally distributed, therefore this process can be repeated in the following time frame. Allowing the premise of normal distribution to be violated by any arbitrary function. Furthermore, optimality is not guaranteed if the distribution is not normal. However, this is not the case with a linear model since a linear combination of two normal distributions is a normal distribution in and of itself. Given these presumptions, the state prediction equation adheres to certain restrictions, which eventually provide positive outcomes. In linearly dynamic systems, the optimal state is estimated using this filter. The same linear Kalman filters, however, can be used in nonlinear systems with a minor adjustment. The Taylor series can be used to linearize the nonlinear system's dynamics at each step of system state estimation.

The linear Kalman filter algorithm is fairly adaptive, allowing it to estimate the states of nonlinear systems as well. We will execute the expanded Kalman filter technique in two stages. Assume that the system's entire information is accessible up to sample $k-1$. This instance involves calculating an initial estimate of the state variables at the sample k based on the mathematical model of the system and the signals available up to time $k-1$. We refer to this Kalman filter stage as the forecast process. Now, of course, the sensors take a new measurement at time k. The second stage of the Kalman filter, known as the update phase, involves improving the first step's prediction using the newly available data to get the final estimated states at the kth sample.

3. Materials and Methods

In this paper, we simulate the data required to estimate the states and outputs. Two types of white Gaussian noise and Poisson noise are added to the output. one kind of statistical noise distinguished by a regularly distributed probability density function is Gaussian noise, sometimes called Gaussian white noise. The noise variance and the mean are the two primary components of Gaussian noise. The noise distribution's mean is centered on the mean; if the mean is zero, the noise distribution's average is the same above and below the mean. Variance quantifies the degree of growth or spread of the noise distribution and shows how far the noise values deviate from or are relative

to the statistical mean. A higher variance indicates that the noise values deviate from the mean, whereas a lower variance indicates that they are around the mean.

The primary cause of image noise, unless in low light, is photon noise, commonly referred to as Poisson noise. It is a basic type of uncertainty whose expected magnitude depends on the signal. The detection of individual photons can be regarded as separate occurrences with a random temporal distribution. The number of photons detected by a particular sensor in a given time interval is therefore represented by a discrete probability distribution, making photon counting a conventional Poisson process.

We consider the covariance matrix as follows:

$$Q = \begin{bmatrix} 0.1 & 0 & 0 & 0 \\ 0 & 0.2 & 0 & 0 \\ 0 & 0 & 0.1 & 0 \\ 0 & 0 & 0 & 0.3 \end{bmatrix}$$

We also add a Gaussian disturbance to the system dynamics, where Q is the covariance of the disturbance.

3.1 *Linear dynamics*

The state space equations for the noisy system are as follows:

$$\dot{X} = Ax + Bu + Gw \tag{11}$$
$$Y = Cx + Du + Hv$$

When the noise in the observation is denoted by v and the dynamical disruption by w. The system dynamics Jacobian concerning the disturbance is G, and the observation Jacobian for the noise is H. A constant value of 0.1 is the input, and the system's initial states are $[0, 0, 0, 1]$. The observation is first subjected to a Gaussian white noise $v \sim N(0,1)$. The noise covariance matrix, denoted as R, is selected in this study in the following manner:

$$R = \begin{bmatrix} 0.1 & 0 \\ 0 & 0.1 \end{bmatrix}$$

The linear system models' observations and simulated states with and without noise and disturbance are displayed in Figure 3. Around zero, the equilibrium point, there is an oscillation between the real position and the angular position.

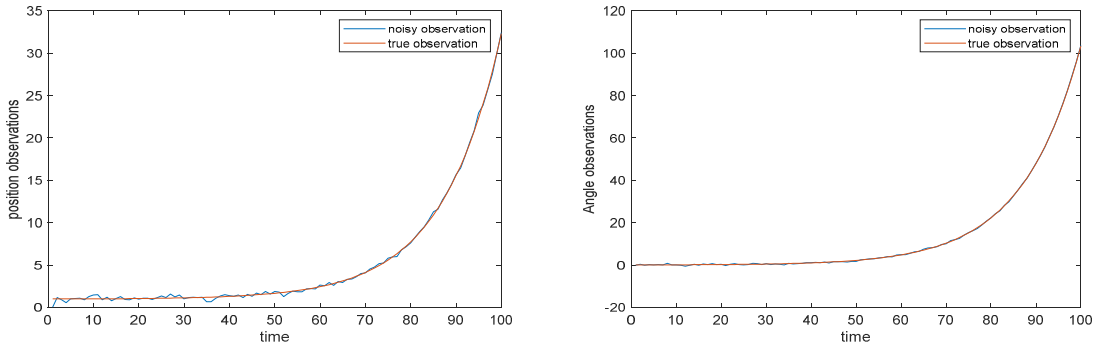

Figure 3. Display of actual position (left) and angular position (right) observations with and without white Gaussian noise in linear dynamics.

We then supplement the output data with a Poisson noise with a value of $\lambda = 0.1$. The states' plots are identical, except the observation plots use Poisson noise rather than Gaussian white noise. Figure 4 displays the graphs of the observations of angular position and real position.

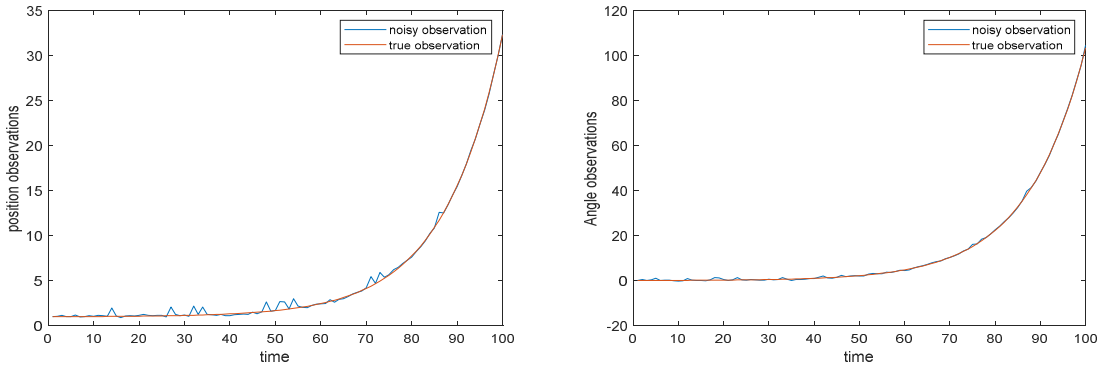

Figure 4. Display of actual position (left) and angular position (right) observations with and without Poisson noise in linear dynamics.

3.2 *Nonlinear dynamics*

Since we are aware that the inverted pendulum is a very nonlinear system, we also construct nonlinear dynamic diagrams of it. The following relationship describes the system's nonlinear equation of state:

$$X = \begin{bmatrix} v \\ 4(0.5(u + w^2 sin\theta) - (0.5x + 0.25cos\theta sin\theta))/(4 - cos^2\theta) \\ w \\ 4(-0.5(sin\theta) + 0.25(cos\theta) - 0.25w^2 cos\theta sin\theta + 0.25xcos\theta))/(4 - cos\theta sin\theta) \end{bmatrix} \quad (12)$$

We simulate observed position and angle measurements with and without noise while maintaining the other parameters constant and the input set to zero. For Gaussian noise, the noisy and true observed values are displayed in Figure 5, and for Poisson noise, they are displayed in Figure 6.

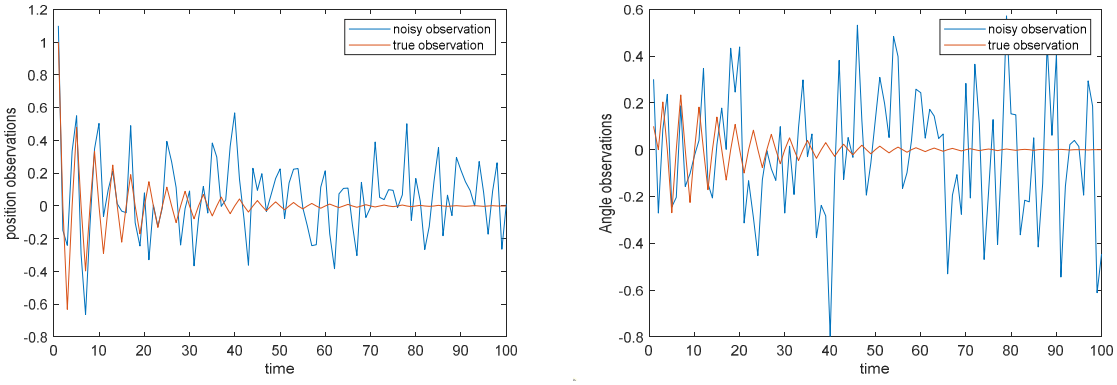

Figure 5. Display of actual position (left) and angular position (right) observations with and without white Gaussian noise in nonlinear dynamics.

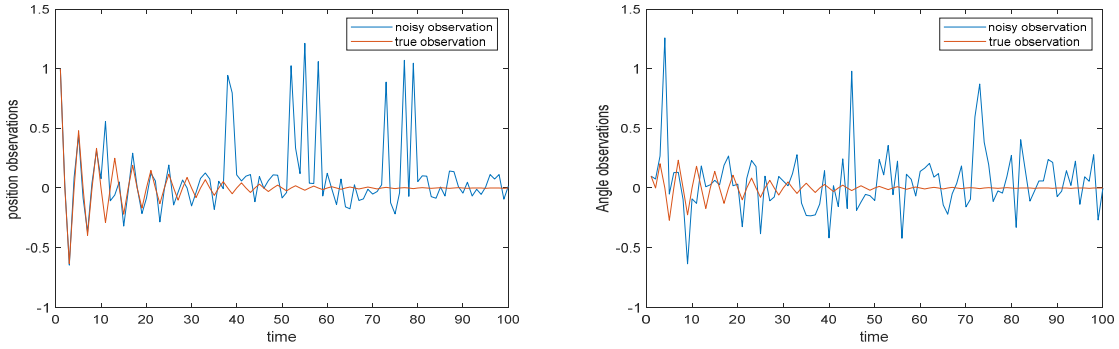

Figure 6. Display of observations of actual position (left) and angular position (right) with and without Poisson noise in nonlinear dynamics.

We see that, in contrast to the linear scenario, the real values do not fluctuate consistently. They exhibit substantial fluctuations at first, but these eventually go away because of the system's nonlinearity. We shall compare the performance of the Kalman filter with the extended Kalman using the nonlinear example. The steady-state estimation error variance is reduced via the Kalman filter. After estimating the process's condition at one point in time, it is given feedback in the form of (noisy) measurements. Two classes of Kalman filter equations are distinguished: To get a previous estimate for the following time step, time update equations (predictor) must estimate the error covariance and forecast the current state (in time). To improve the posterior estimate, measurement update equations (corrector) are in charge of providing feedback by adding a new measurement to the previous estimate. For prediction, we look at a system with a temporal constant. The estimated error J, which is determined by, minimizing using the Kalman gain matrix L.

$$J = y - \hat{y}$$

where y represents the measured value and $\hat{y}$ Represents the estimated value. According to the following algorithm, the states that are updated by the algorithm and approximated using the system's time-constant dynamics are implemented (Figure 7).

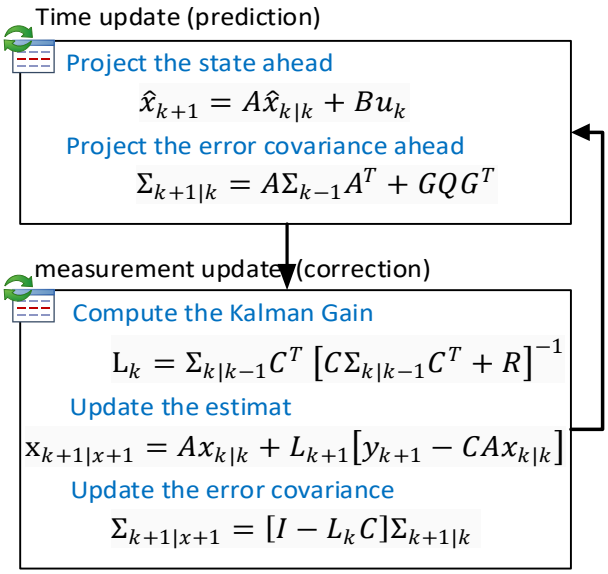

Figure 7. Proposed algorithm for Kalman and extended Kalman filter performance in nonlinear dynamics

A solution to the nonlinear filtering problem is the extended Kalman filter. The Jacobian of the system is found to linearize the dynamics and output functions at the present step.

$$A_t = \frac{\partial f_t}{\partial x}(\hat{x}_{t|t})$$

$$C_t = \frac{\partial h_t}{\partial x}(\hat{x}_{t|t-1})$$

$$G_t = g_t(\hat{x}_{t|t})$$

An approximation of conditional probability and covariance is then carried out in each time step. The following describes the steps involved in the Kalman filter:

$$\hat{x}_{t|t} = \hat{x}_{t|t-1} + L_t(y_t - h_t(\hat{x}_{t|t-1}))$$

$$\hat{x}_{t+1|t} = f_t(\hat{x}_{t|t}))$$

$$L_t = \Sigma_{t|t-1} C_t{}^T \left[C_t \, \Sigma_{t|t-1} C_t{}^T + R_t\right]^{-1}$$

$$\Sigma_{t|t} = \Sigma_{t|t-1} - \Sigma_{t|t-1} C_t{}^T \left[C_t \, \Sigma_{t|t-1} C_t{}^T + R_t\right]^{-1} C_t \Sigma_{t|t-1}$$

$$\Sigma_{t|t} = A_t \, \Sigma_{t|t} A_t{}^T + G_t \, \mathrm{Q}_t G_t{}^T$$

According to the aforementioned relations, the measurement update equations correct the state and covariance estimates with the y_t Measurement and the time update equations display the state and covariance estimates from the previous time step $k-1$ to the present time step k.

4. Results and Discussion

Figure 8 displays the outcomes for Poisson noise using Kalman and extended Kalman filters. For convenience, all dynamical constants are taken to have unit values. Figure 9 displays the findings for angular observations, whereas Figure 8 displays the values of the Kalman filter and the extended Kalman for position observations, respectively.

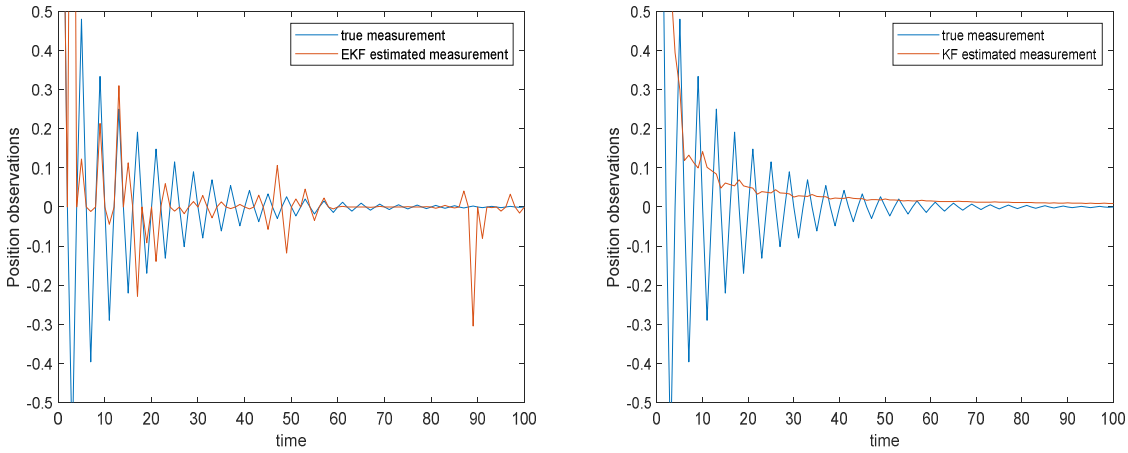

Figure 8. Position observation results obtained from Kalman and extended Kalman filters in nonlinear dynamics and the presence of Poisson noise.

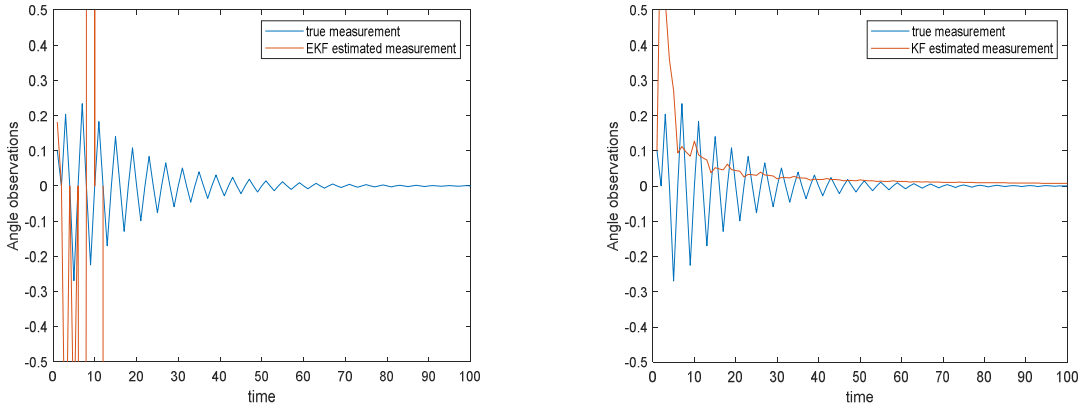

Figure 9. Angular observation results obtained from Kalman and extended Kalman filters in nonlinear dynamics and the presence of Poisson noise.

Figures 10 and 11 display the noise results produced using Kalman and extended Kalman filters. The Kalman filter and extended Kalman filter values for position observations are displayed in the graphs in Figure 10, while the results for angular observations are shown in the graphs in Figure 11.

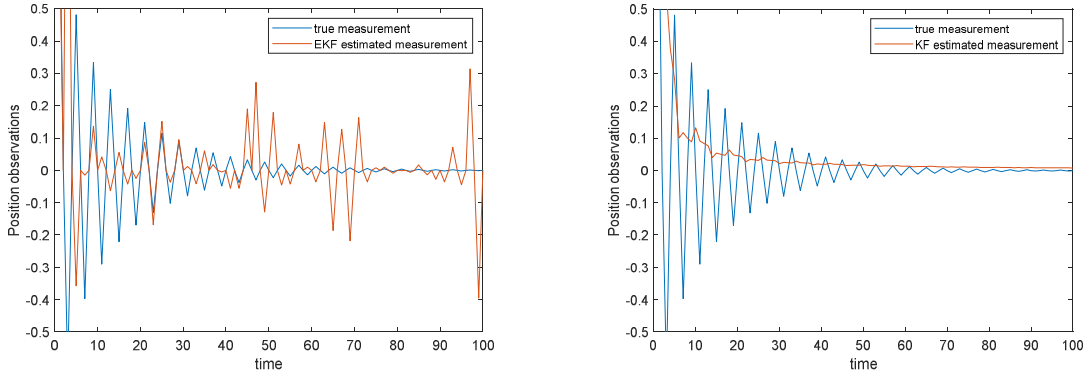

Figure 10. Position observation results obtained from Kalman and extended Kalman filters in nonlinear dynamics and the presence of Gaussian noise.

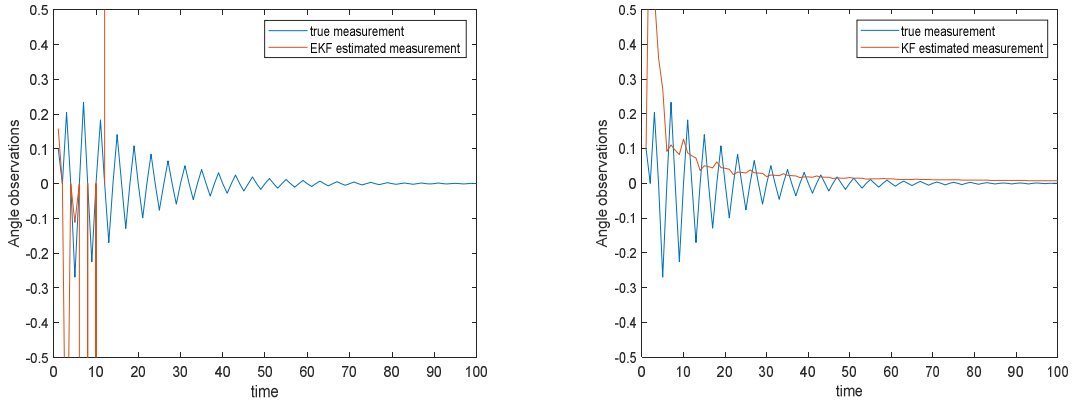

Figure 11. Angular observation results obtained from Kalman and extended Kalman filters in nonlinear dynamics and the presence of Gaussian noise.

The extended Kalman filter produces a first-order linear approximation of the nonlinear dynamics at each time step, which is why we observe that it converges to the real values more effectively. As a result, the mean and covariance converge far more quickly than in the Kalman example, when the mean and covariance are determined using a linear model. We observe that, in contrast to the Gaussian noise scenario, the Kalman filter does not significantly alter Poisson noise. Comparing the extended Kalman filter to the Gaussian noise scenario, the latter takes longer to converge to the real value. After convergence, it fluctuates once more in certain instances. The noise covariance matrix can be changed to enhance performance. However, in the case of Gaussian white noise, the extended Kalman filter performs worse. We can use the unscented Kalman filter or the particle filter when we employ different initial conditions because even the extended Kalman filter might not be enough to get estimates that are near the genuine values. When the dynamics of the system exhibit significant nonlinearity, they are employed. Furthermore, in comparison to the Kalman filter, the extended Kalman filter is not very good.

4. Conclusions

In this research, we focused on the IPS problem and found that even the extended Kalman filter may not be sufficient to obtain estimates close to the true values, and therefore we can turn to other methods. They are used for cases where there is a large amount of nonlinearity in the system dynamics. We observed that the performance of the Kalman filter in Gaussian noise and Poisson noise is not much different, and also in Poisson noise, it converges to the real value in a longer time compared to Gaussian noise. We can improve the performance of the Kalman filter by adjusting the noise covariance matrix. Indeed in extended Kalman filter, as observed for white Gaussian noise, good performance was not achieved in Poisson noise. We also noticed that in extended Kalman filter, convergence to real values was not achieved or it converged to real values with large fluctuations. It should also be noted that the extended Kalman filter is not good compared to the Kalman filter.

Conflicts of Interest

The author declares that there are no conflicts of interest regarding this article.

References

1. Jie Z, Sijing R. Sliding mode control of inverted pendulum based on state observer. In 2016 Sixth International Conference on Information Science and Technology (ICIST). 2016, 322-326.
2. Shimada A, Yongyai C. Motion control of inverted pendulum robots using a kalman filter based disturbance observer. *SICE J. Control Meas. Syst. Integr.* 2009, 2(1), 50-55.
3. Marrison CI, Stengel R F. Design of Robust Control Systems for a Hypersonic Aircraft. *J. Guid. Control Dyn.* 1998, 21(1), 58-63.
4. Yao B, Al-Majed M, Tomizuka M. High-performance robust motion control of machine tools: an adaptive robust control approach and comparative experiments. *IEEE/ASME Trans. Mechatron.* 1997, 2(2), 63-76.
5. Housner GW. The behavior of inverted pendulum structures during earthquakes. *Bull. Seismol. Soc. Am.* 1963, 53(2), 403-417.
6. Wang JJ. Simulation studies of inverted pendulum based on PID controllers. *Simul. Model. Pract. Theory* 2011, 19(1), 440-449.

7. Li D, Chen HS, Fan J, Shen C. A novel qualitative control method to inverted pendulum systems. *IFAC Proc. Vol.* 1999, 32(2), 1495-500.
8. Nasir ANK, Razak AAA. Opposition-based spiral dynamic algorithm with an application to optimize type-2 fuzzy control for an inverted pendulum system. *Expert Syst. Appl.* 2022, 195, 116661.
9. Tsay SC, Fong IK, Kuo TS. Robust linear quadratic optimal control for systems with linear uncertainties. *Int. J. Control* 1991, 53(1), 81-96.
10. Lin F. An optimal control approach to robust control design. *Int. J. Control* 2000, 73(3), 177-186.
11. Zhang X, Kamgarpour M, Georghiou A, Goulart P, Lygeros J. Robust optimal control with adjustable uncertainty sets. *Automatica* 2017, 75, 249-259.
12. Wang D, Liu D, Zhang Q, Zhao D. Data-based adaptive critic designs for nonlinear robust optimal control with uncertain dynamics. *IEEE Trans. Syst. Man Cybern. Syst.* 2015, 46(11), 1544-1555.
13. Bellman R. Dynamic Programming. *Science* 1966, 153(3731), 34-37.
14. Pontrjagin LS, Gamkrelidze RV. The mathematical theory of optimal processes. New York: Gordon and Breach, 1986.
15. Powell WB. Approximate dynamic programming: solving the curses of dimensionality. Hoboken: John Wiley & Sons, 2011.

How to cite this article: Pourmir M. Optimization of the State of an Inverted Pendulum System Using Kalman Filter in the Presence of Gaussian and Poisson Noise. *Curr. Appl. Sci.*, 2025, 3(2):61-72. https://doi.org/10.22034/cas.2025.496057.1045